

# CHORUS

This is the accepted manuscript made available via CHORUS. The article has been published as:

## Experimental study of ac Josephson effect in gate-tunable $(\text{Bi}_{1-x}\text{Sb}_x)_2\text{Te}_3$ thin-film Josephson junctions

Yuusuke Takeshige, Sadashige Matsuo, Russell S. Deacon, Kento Ueda, Yosuke Sato, Yi-Fan Zhao, Lingjie Zhou, Cui-Zu Chang, Koji Ishibashi, and Seigo Tarucha

Phys. Rev. B **101**, 115410 — Published 11 March 2020

DOI: [10.1103/PhysRevB.101.115410](https://doi.org/10.1103/PhysRevB.101.115410)

# Experimental study of ac Josephson effect in gate-tunable $(\text{Bi}_{1-x}\text{Sb}_x)_2\text{Te}_3$ thin film Josephson junctions

Yuusuke Takeshige,<sup>1</sup> Sadashige Matsuo,<sup>2,3,\*</sup> Russell S. Deacon,<sup>2,4</sup> Kento Ueda,<sup>1</sup> Yosuke Sato,<sup>1</sup> Yi-Fan Zhao,<sup>5</sup> Lingjie Zhou,<sup>5</sup> Cui-Zu Chang,<sup>5</sup> Koji Ishibashi,<sup>2,4</sup> and Seigo Tarucha<sup>2,†</sup>

<sup>1</sup>*Department of Applied Physics, The University of Tokyo, 7-3-1 Hongo, Bunkyo, Tokyo 113-8654, Japan*

<sup>2</sup>*Center for Emergent Matter Science, RIKEN, 2-1 Hirosawa, Wako-shi, Saitama 351-0198, Japan*

<sup>3</sup>*JST, PRESTO, 4-1-8 Honcho, Kawaguchi, Saitama, 332-0012, Japan*

<sup>4</sup>*Advanced Device Laboratory, RIKEN, 2-1 Hirosawa, Wako-shi, Saitama 351-0198, Japan*

<sup>5</sup>*Department of Physics, Pennsylvania State University, University Park, Pennsylvania 16802, USA*

We report on measurements of the ac Josephson effect in three-dimensional topological insulator (TI) Josephson junctions with Fermi energy tuning using a back gate. We successfully tune the Fermi energy into the bulk gap of the TI. We observe that the Josephson energy as a function of the gate voltage has a dip feature, indicating the presence of specular Andreev reflections. We study the ac Josephson effect with detection of both Shapiro steps and Josephson emission. The obtained results show no signature of Majorana modes. With the support of simulations, we conclude that the observation of the fractional ac Josephson effect may be complicated by both a large parallel capacitance and a small ratio of current carried in  $4\pi$  period modes compared to conventional  $2\pi$  modes.

## INTRODUCTION

Majorana Fermions (MFs) were discovered as one of the solutions to the Dirac equation by Ettore Majorana in 1937<sup>1</sup>. After decades, Alexei Kitaev proposed that MFs can appear at the edge of a spin-less one-dimensional superconductor<sup>2</sup>. This proposal has promoted research of the MFs in condensed matter physics, especially in order to reveal the non-abelian statistics and possible application to topological quantum computation<sup>3-5</sup>. One of the platforms for generating MFs is to engineer topological superconductivity<sup>2</sup> in hybrid superconducting systems. Until now, superconducting junctions such as junctions of semiconductor nanowires<sup>6,7</sup>, topological insulators (TIs)<sup>8,9</sup> have been proposed theoretically. Experimentally, signatures of MFs such as localized zero-energy modes<sup>10-12</sup>, exponential protection of the localized modes<sup>13</sup> and  $4\pi$  periodic Josephson supercurrent<sup>14-21</sup> have been observed. In addition to the junctions mentioned above, ferromagnetic atoms on superconductors also have shown the localized zero-energy modes<sup>22,23</sup>, and superconducting junctions of Dirac semimetals have also shown evidence of the  $4\pi$  periodic Josephson supercurrent<sup>24,25</sup>.

In superconducting junctions of semiconductor nanowires or ferromagnetic atoms, a strong magnetic field or ferromagnetism are required for the most cases of engineering of MFs, resulting in soft superconducting gap which degrades topological protection of MFs. However, the TI-superconductor junctions do not need such a strong magnetic field or ferromagnetism. **We note that we need the weak magnetic fields to induce the vortices holding the localized MFs in the systems<sup>26,27</sup>.** For the two-dimensional TI Josephson junction (JJ), the ac Josephson effect has been studied with Fermi energy tuning<sup>16,17</sup>. On the contrary, all the previous reports on ac Josephson effect of three-dimensional (3D) TI JJs do

not address Fermi energy tuning<sup>15,18-20,28</sup>, meaning that the bulk contributions possibly remain. Therefore, it is important to demonstrate that the surface states are essential for observations of a fractional ac Josephson effect that indicates Majorana modes. Furthermore, routes toward electrical control and braiding of MFs in 3D TI based systems have been proposed<sup>27,29</sup> allowing MFs engineered in superconducting junctions of 3D TI to be utilized for demonstration of the non-Abelian statistics. This is the additional motivation to study 3D TIs JJs.

Here we show experimental results of JJs with weak links formed from gate tunable  $(\text{Bi}_{1-x}\text{Sb}_x)_2\text{Te}_3$  (BST) thin films. We succeed in electrical control of normal resistance ( $R_n$ ) and switching current ( $I_{sw}$ ) of the JJs. We find that the observed  $I_{sw}R_n$  shows a dip feature near the charge neutral point assigned to the analog of specular Andreev reflection. We measure the Shapiro steps of the JJ and observe that both odd and even integer-multiple Shapiro steps appear even around the charge neutral point with no evidence of fractional ac Josephson effect. Additionally, we measured Josephson emission and detect a conventional spectra which is also contrary to the prediction for junctions with Majorana modes. We discuss possible reasons why the measured ac Josephson effect is conventional.

We choose BST as a 3D TI because the topological nature has already been demonstrated by ARPES measurements<sup>30</sup> and also the features of Dirac electrons on the surface have been reported in electron transport experiments of, for example, Shubnikov de Haas oscillations<sup>31</sup> and the quantum Hall effects<sup>32</sup>. In addition, the Fermi energy of BST can be tuned by chemical doping and also electric-field tuning. We use a thin film of  $(\text{Bi}_{1-x}\text{Sb}_x)_2\text{Te}_3$  ( $x = 0.8$ ) grown on heat-treated  $\text{SrTiO}_3$  substrate (111) by molecular beam epitaxy. The thickness of the  $(\text{Bi}_{1-x}\text{Sb}_x)_2\text{Te}_3$  is 8 quintuple layers (8 nm) and the out-of plane direction is (111). **This is thick**

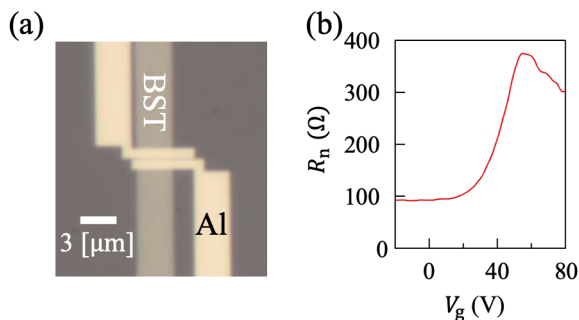


FIG. 1. (a) The top view of Sample A. (b) The  $V_g$  dependence of the  $R_n$ .  $R_n$  is defined as an average of differential resistance obtained at  $I$  larger than  $I_{sw}$ .

enough to avoid the hybridization of the top and bottom surface states<sup>30</sup>. The SrTiO<sub>3</sub> substrate is 0.5 mm thick. We can tune the Fermi energy electrically by applying gate voltage on the back of the substrate.

We fabricated this BST films into JJs devices. The mesas were patterned by Ar ion etching and superconducting contacts were fabricated with conventional electron beam lithography and metal deposition. Before the metal deposition, we dipped the sample in diluted HCl to remove the oxidized surface layer<sup>33</sup>. Next, we deposited Ti (0.5 nm)/ Al (30 nm) for Sample A and MoRe (80 nm) for sample B, respectively. An optical image of sample A is shown in Fig. 1 (a). Electrical measurements were carried out in a dilution refrigerator with base temperature of 30 mK. We executed 4-terminal measurements with DC current bias.

## EXPERIMENTAL RESULTS

First, we focus on gate voltage ( $V_g$ ) dependence of  $R_n$  of Sample A. Figure 1 (b) shows the  $R_n$ - $V_g$  plot. A peak of  $R_n$  can be seen at  $V_g \approx 55$  V, indicating the charge neutral point. Next the  $V_g$  dependence in the superconducting region is studied. Figure 2 (a) shows the differential resistance as a function of  $V_g$  and current ( $I$ ) for Sample A. The zero-resistance region around bias current  $I = 0$  nA indicates that the supercurrent flows through the JJ. The sharp  $dV/dI$  peak (white lines) when the current increases indicates the switching of the junction from super (black) to normal (blue) branches. Here  $V$  is the measured voltage. We define the switching current  $I_{sw}$  as  $I$  at the sharp peak with  $I > 0$ . Since  $I_{sw}$  strongly depends on  $V_g$  and  $R_n$ , it is concluded the supercurrent can be controlled by the gate voltage. This guarantees that the supercurrent flow through the BST film.

Figure 2 (b) shows the  $dV/dI$  as a function of  $I$  and a magnetic field perpendicular to the film ( $B$ ) at  $V_g = 0$  V. The  $B$  dependence of  $I_{sw}$  approximately follows the Fraunhofer pattern which is usually observed in conventional planar JJ devices. This result also sup-

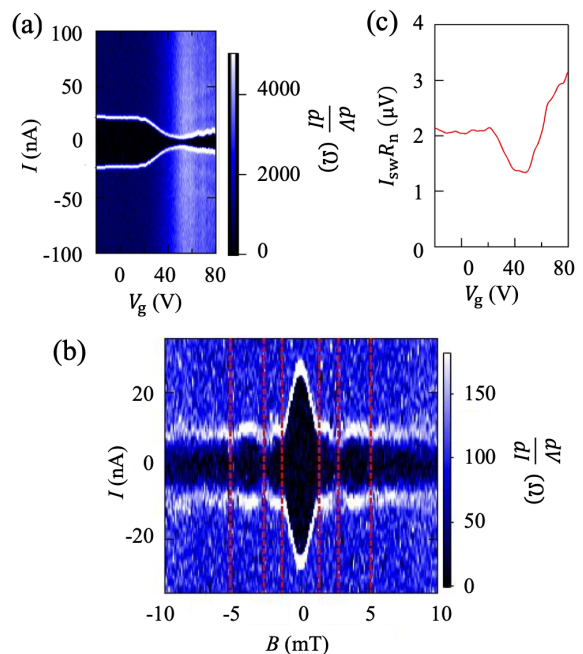


FIG. 2.  $V_g$  and  $I$  dependence of differential resistance (a). (b) Bias current and the magnetic field dependence of differential resistance. Red dashed lines indicate the nodes' positions of Fraunhofer pattern. (c)  $V_g$  dependence of  $I_{sw}R_n$ , dip feature appears near the charge neutral point.

ports that the supercurrent flows through the BST films. However, there are two unexpected features found in the magnetic field dependence. First, the intervals between nodes as indicated by the red dashed lines are not constant. Second,  $I_{sw}$  does not become 0, even at the node point. These features can indicate a non-uniform supercurrent distribution because the magnetic field dependence can take a shape of a sum of Fraunhofer patterns having different periods. In this case the intervals cannot be constant and a finite supercurrent can remain even at the nodes. The junction area calculated from the junction geometry is  $0.3 \mu\text{m}^2$ , which is inconsistent with the area of  $0.81 \mu\text{m}^2$  evaluated from the distance between second and third nodes. Similar inconsistency has been previously assigned to the flux focusing effect<sup>34,35</sup>.

We now provide further discussion on the  $V_g$  dependence in terms of the Josephson energy. From the result of Fig. 2 (a), we calculate the product  $I_{sw}R_n$  at each  $V_g$  as shown in Fig. 2 (c). The value of  $I_{sw}R_n$  is of the order of a few  $\mu\text{V}$ , which is much smaller than the Al superconducting gap  $\approx 170 \mu\text{V}$ , indicating poor transparency of the BST/Al interface. The evaluated  $I_{sw}R_n$  has a dip feature around  $V_g \approx 55$  V. In JJs of other 3D TIs or graphenes, similar dip features have been reported in the gate dependence of  $I_{sw}R_n$ <sup>33,36–41</sup>. We attribute this dip to the influence from the electron-hole puddles, the locally distributed p or n doped regions that appear near the charge neutral point due to inhomogeneity. The transport phenomena related to the puddles

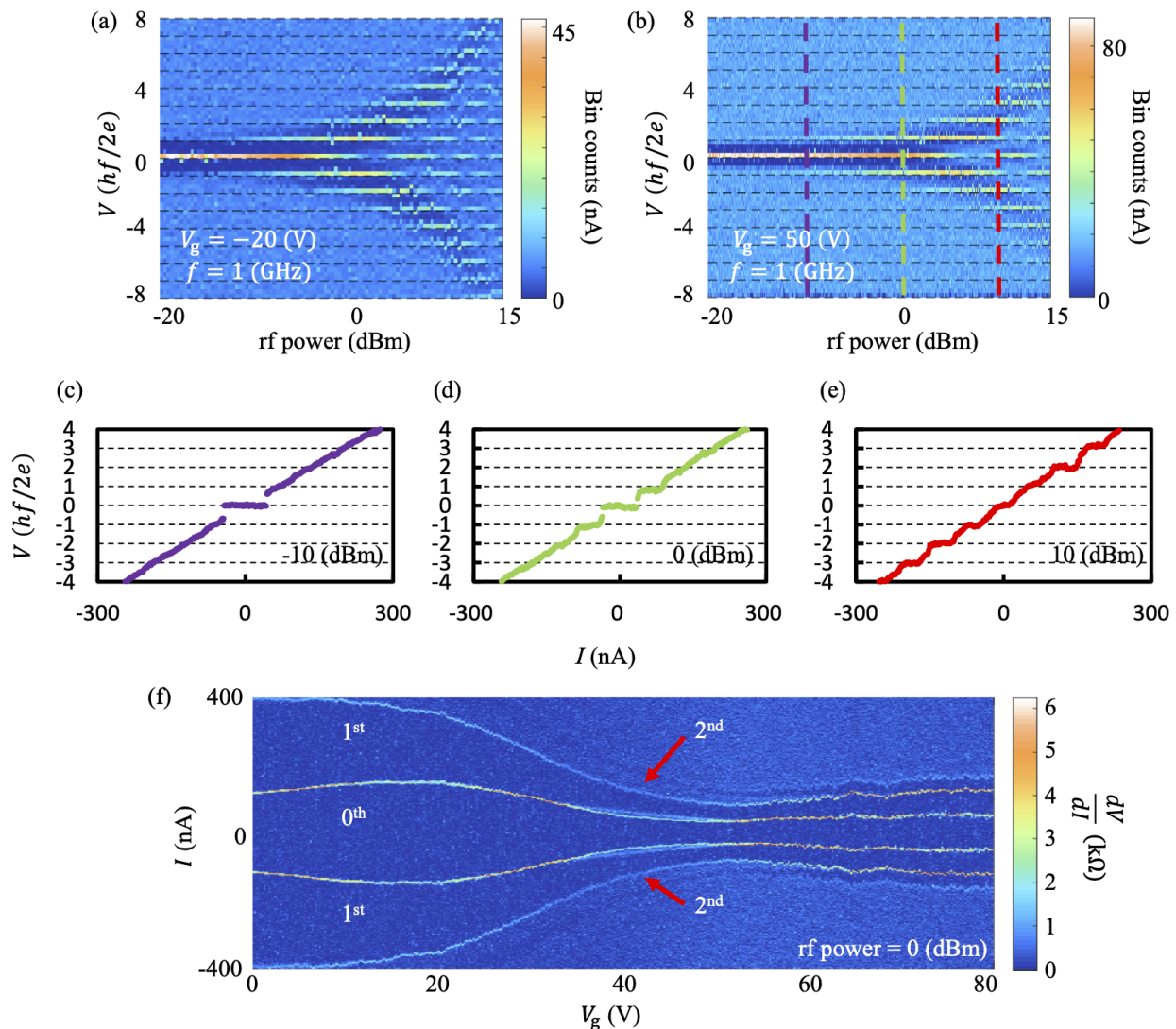


FIG. 3. Shapiro steps of Sample A with  $V_g = -20$  V (a), and  $V_g = 50$  V (b). In both data sets the first steps appear clearly. (c)-(e) Shapiro step measurements along each dashed lines in (b). The colors of each graphs correspond to the color of dashed lines in (b). (f)  $V_g$  dependence of the Shapiro steps in Sample A showing that the first step appears for the full range of gate voltage studied. In all cases a used frequency is 1 GHz.

has been intensively studied in graphene devices, both theoretically and experimentally, for example<sup>42–46</sup>. The  $I_{sw}$  suppression<sup>46</sup> can be attributed to the charge scattering at the boundaries of electron-hole puddles taking the form of specular Andreev reflections<sup>47</sup>. This specular Andreev reflection does not have the retro-reflection property of Andreev events, causing reduction of  $I_{sw}R_n$  near the charge neutral point<sup>46</sup> than in the carrier-doped regions. Existence of the puddles are observed also in 3D TIs<sup>48</sup> and the specular Andreev reflection is theoretically predicted on the interface of 3D TI and a superconductor<sup>49</sup>. Therefore, the same scenario can work for the  $I_{sw}R_n$  suppression near the charge neutral point as shown in Fig. 2 (c). We note that the  $I_{sw}R_n$  reduction can be ascribed to fluctuation<sup>37–40</sup>, or ripples<sup>41</sup>. Sample A, however, has small hysteresis<sup>50</sup>. This indicates

that the difference between the measured switching current and critical current does not play an important role in Sample A. In addition, Our sample is not monolayer, and therefore should contain less ripples. Finally, we conclude that the observed  $I_{sw}R_n$  dip feature arises from the electron-hole puddles.

We next move to the measurement results of  $V$  vs. current  $I$  while irradiating rf microwave excitation to the JJ. Binning<sup>15</sup> method is used to evaluate the Shapiro steps. Measured DC voltage is converted to the histogram of the voltage for each  $I$  in bins of  $0.25 \times hf/2e$ . As source current is swept at a constant rate the counts per bin reflect the current on a given Shapiro step. Figures 3 (a) and (b) show the bin counts of the measurement as a function of rf power of the microwave at  $V_g = -20$  V and 50 V respectively. The histogram is expected to show peaks

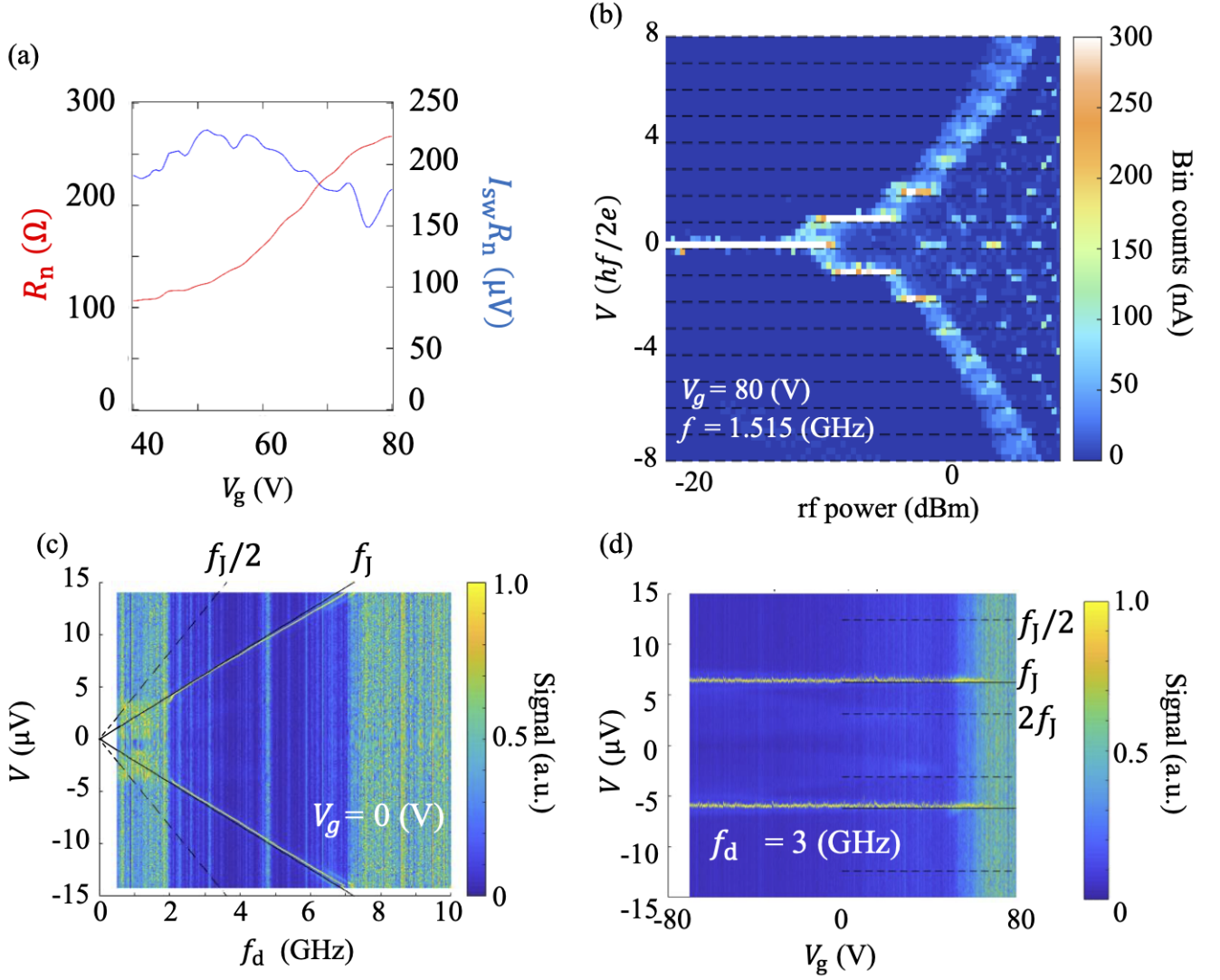


FIG. 4. Measurement of the Josephson effects for Sample B: (a)  $V_g$  dependence of  $R_n$  and  $I_{sw}R_n$  of Sample B. (b) The Shapiro steps at  $V_g = 80$  V. (c) The measured Josephson emission at  $V_g = 0$  V. The dark solid line indicates  $f_J$  and dashed line indicates  $f_J/2$  respectively. A strong emission feature is only seen at  $f_J$  with weak signature of higher harmonics around  $2f_J$ . (d)  $V_g$  dependence of Josephson emission. The resonance only occur at the frequency is  $f_J$  and weakly at  $2f_J$ . Here dark solid line is  $f_J$  and dashed lines are  $f_J/2$  or  $2f_J$ .

originated from the Shapiro steps at quantized voltages of multiples of  $hf/2e$  in conventional JJs and odd number multiples would disappear in topological JJs. Here  $h$  is the Planck's constant,  $f$  is the irradiated microwave frequency, and  $-e$  is the electron charge. In Figs. 3 (a) and (b), all Shapiro steps including the odd number steps appear clearly. The steps can also be observed in  $I - V$  curves of Fig. 3 (c)-(e) which corresponds to the cuts of Fig. 3 (b). Colors of graphs are the same as the color of dashed line in Fig. 3 (b). Figure 3 (f) shows the  $dV/dI$  as a function of  $V_g$  and bias current. The first step appears at all gate voltages. This indicates that the fractional ac Josephson effect is not observed in this JJ.

One possible reason why the odd number Shapiro steps remain is the small  $I_{sw}R_n$ . According to the preceding

researches<sup>15,51</sup>, in order to observe the vanishing of the odd number Shapiro steps in coexistence of both  $4\pi$  and  $2\pi$  periodic components with dominant  $2\pi$  modes, the microwave frequency should satisfy a condition of

$$f < (2eI_c^{4\pi}R_n)/h \quad (1)$$

Here  $I_c^{4\pi}$  is the critical current of the  $4\pi$  periodic component. In our case, assuming a possibility of a low contribution in the supercurrent from the  $4\pi$  periodic modes combined with the small  $I_{sw}R_n$  we consider that the vanishing odd number steps would only be observed for a low frequency range. Since the Shapiro step signals become weaker as the frequency is lowered, it becomes difficult to measure well resolved features.

To increase  $I_{\text{sw}}R_n$ , we use Sample B with MoRe as the contact superconductor. MoRe has a larger superconducting gap than Al so that a larger  $I_{\text{sw}}R_n$  is expected. The measured  $R_n$  vs.  $V_g$  is shown as a red line in Fig. 4 (a).  $R_n$  increases monotonically with  $V_g$  and then starts to saturate around  $V_g = 80$  V. This saturation behavior implies that the BST at  $V_g = 80$  V is around the charge neutral point. The calculated  $I_{\text{sw}}R_n$  is around  $180 \mu\text{V}$  in  $V_g = 80$  V, shown as a blue line in Fig. 4 (a). This result means the upper limit described in Eq. 1 of the MoRe JJs is almost 100 times larger than the Al JJs.

Then we move to the analysis of Shapiro steps. Here irradiated microwave frequency is  $f = 1.515$  GHz. The result as a function of bias voltage and the rf power is shown in Fig. 4 (b). The first step clearly appears.

**We also measured the Josephson emissions of sample B in our emission measurement setup<sup>17</sup>.** With applying bias voltage  $V$ , the intensity of the emitted microwave from the JJ at each detection frequency ( $f_d$ ) is analysed. Measurements performed at each detection frequency have a background subtraction, taken as the amplitude at zero current and are normalized by the peak amplitude at that frequency. Emission features at  $f_J = 2eV/h$  and  $f_J/2 = eV/h$  are expected from conventional and topological JJs, respectively. Figure 4 (d) shows the gate voltage dependence of the emitted RF signal at  $f_d = 3$  GHz. The dark solid and dashed lines indicate  $f_J$  and  $f_J/2$  or  $2f_J$ , respectively. Even in this case the observed resonance is seen only in  $f_J$ . The emission signal is observed only at  $f = f_J$  with a weak second harmonic feature around  $2f_J$  for some gate voltages.

One possible reason why we are unable to observe vanishing odd number Shapiro steps and appearance of  $f_J/2$  emission may be the large parallel capacitance ( $\simeq 100$  pF) originating from the huge dielectric constant of SrTiO<sub>3</sub> substrate. In fact, preceding theoretical research indicates that high junction capacitance can complicate the observation of the missing of Shapiro steps<sup>52</sup>. In addition, we also speculate that a small  $4\pi$  periodic current contribution is preventing the detection of fractional Josephson effect. We discuss these points based on numerical simulation below.

## DISCUSSIONS

The salient features of the ac Josephson effect in a weak link with both  $4\pi$  periodic and  $2\pi$  periodic modes were described by Dominguez *et al.* using a two periodicity resistively shunted Josephson junction model<sup>51</sup>. More recently, the two periodicity model has been expanded to more completely capture the behavior of real devices. For example, the effect of Joule heating<sup>18</sup> and capacitance<sup>52</sup> have been investigated. The resistively capacitively shunted junction (RCSJ) model including the two components of  $2\pi$  and  $4\pi$  periodic supercurrent is based on the simple current biased circuit which is depicted in Fig. 5 (a). Time evolution of the phase difference,  $\phi$  is

written as

$$\frac{C}{I_c} \frac{\hbar}{2e} \frac{d^2\phi}{dt^2} + \frac{\hbar}{2e} \frac{1}{RI_c} \frac{d\phi}{dt} + \frac{i_{\text{sc}}(\phi)}{I_c} = \frac{1}{I_c} (i_0 + i_1 \sin(\omega_{\text{ac}}t)), \quad (2)$$

where  $\hbar$  is Dirac's constant,  $C$  is the junction capacitance,  $R$  is the resistance including the junction resistance  $R_{\text{JJ}}$  and a parallel shunt resistance  $R_{\text{shunt}}$ ,  $I_c$  is critical current of JJ, and  $i_0$  is the external current bias. Variable  $i_{\text{sc}}(\phi)$  is the current phase relationship of the entire junction which is comprised of two components with different periodicity,  $i_{\text{sc}}(\phi) = i_{2\pi} \sin(\phi) + i_{4\pi} \sin(\phi/2)$ . Here, we consider the value of  $r = i_{4\pi}/i_{2\pi}$ . We also define Stewart McCumber parameter  $\beta_c = (2eR^2I_cC)/\hbar$ . We assume that  $i_{4\pi} \ll i_{2\pi}$ , because only electrons whose incident angle is perpendicular to the interface between the superconductors and BST contribute to the  $4\pi$  periodic component<sup>8</sup>. Here we consider only Josephson emission for simplicity. So we focus on the case with no external drive such that  $i_1 = 0$ .

For each set of device parameters we solve the RCSJ model and perform a fast fourier transform (FFT) calculation of  $\phi(t)$  traces to extract plots like that shown in Fig. 5 (b). We then extract the amplitude of Josephson emission,  $A_{2\pi}$  and  $A_{4\pi}$  at  $f_J$  and  $f_J/2$ , respectively.

We consider the effects of variation of  $R_{\text{shunt}}$ ,  $C$  and  $r$  in Fig. 6. Since changing  $R_{\text{shunt}}$  is equal to changing  $\beta_c (\propto C)$ , we focus on the value of  $\beta_c$  and  $r$ . Fig. 6 shows the ratio of  $A_{2\pi}$  and  $A_{4\pi}$  for different  $\beta_c$  and  $r$ . For high frequency all data sets in Fig. 6 (a) collapse to a single line indicating that the ratio of emission amplitudes is determined by the ratio  $r$ . We can also see the crossover in very low frequency region ( $f_J \ll 5$  GHz) in which  $A_{4\pi}/A_{2\pi}$  abruptly becomes large and reaches at 1. This indicates the crossover from the purely  $4\pi$  regime to the  $4\pi + 2\pi$  regime<sup>53</sup> as the frequency becomes high. In contrast, as capacitance becomes larger (equal to higher  $\beta_c$ ), this crossover becomes lower frequency as shown in Fig. 6 (b). This means that in the high  $C$  case, the purely  $4\pi$  periodic region is difficult to access. We also see the effect of  $r$ . Lowering  $r$  decreases the relative emission amplitudes for large  $f_J$  as illustrated in Fig. 6 (c). In the case that  $r$  is less than 0.1, the ratio  $A_{4\pi}/A_{2\pi}$  is much smaller than  $r$ . This indicates  $A_{4\pi}/A_{2\pi}$  is further reduced for small  $r$ . Though our calculations make some features of Josephson emission clear, there may be other mechanisms such as Joule heating and quasi particle poisoning of the  $4\pi$  periodic states<sup>18</sup> which are not captured in the RCSJ model used here.

We can assume that due to the high junction capacitance and possible resulting sizeable  $\beta_c$ , the crossover regime between the purely  $4\pi$  periodic and mixed dynamics is inaccessible. Therefore we are accessible to only the high bias regime in which the amplitude of the  $f_J/2$  feature would reflect the relative contribution of the  $4\pi$  periodic component in the current phase relationship. Assuming the minimum of a single channel with perfect transmission due to a Majorana mode and a

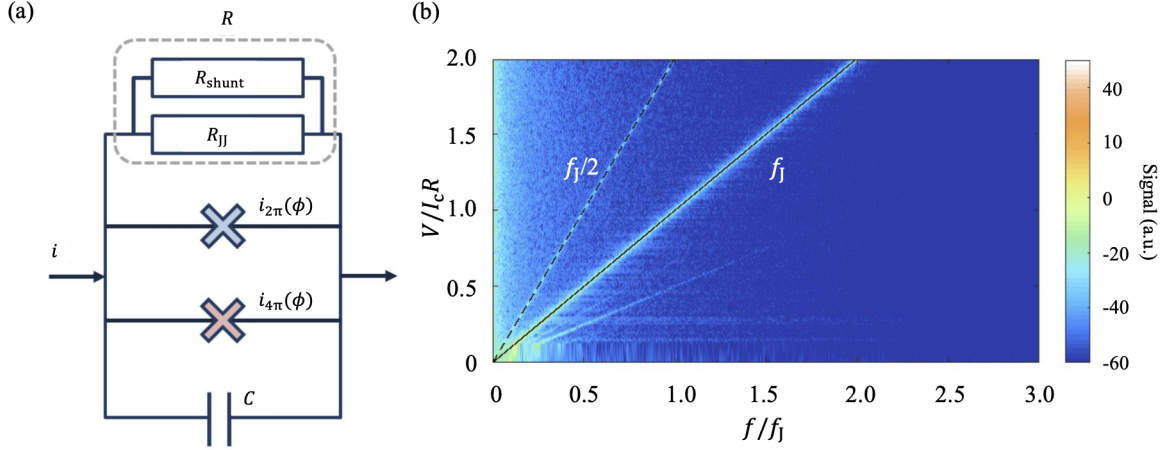


FIG. 5. (a) The circuit diagram of the RCSJ model. (b) Example simulation results for  $r = 0.15$  and  $\beta_c = 10$ . Black line indicates  $f_J$  emission, and black dashed line indicates  $f_J/2$  emission.

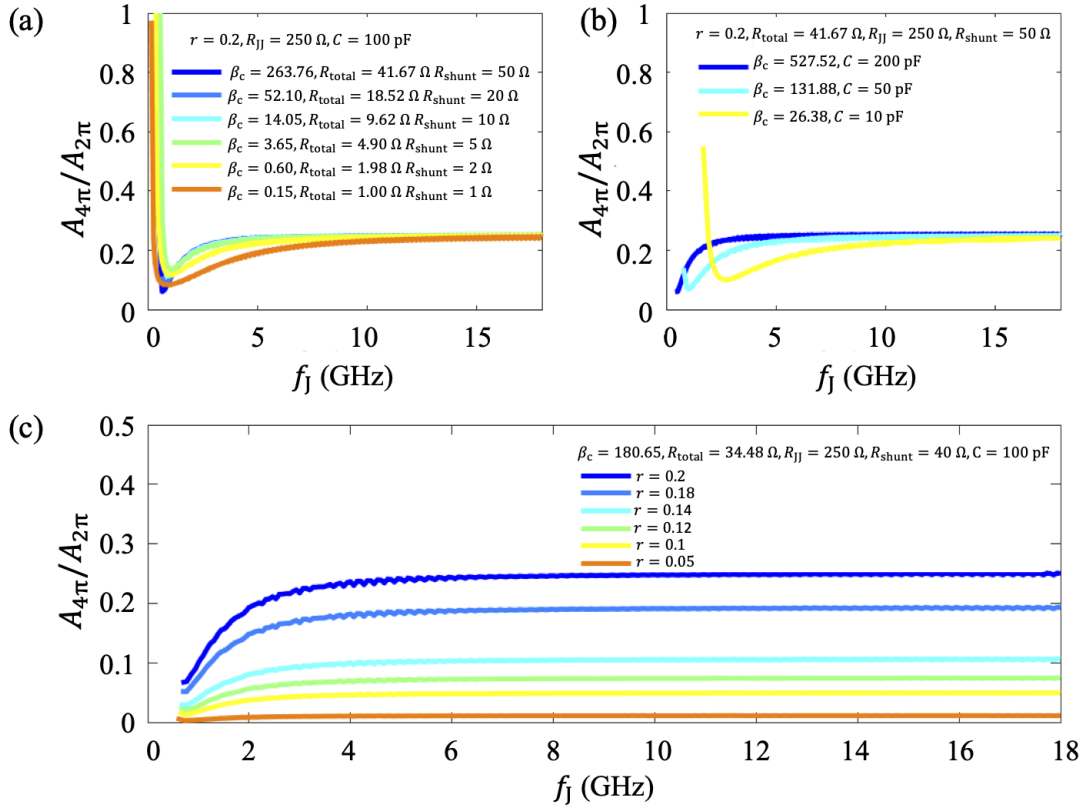


FIG. 6. (a) Simulation results for different  $R_{\text{shunt}}$  with  $r = 0.2$ . This is equal to change  $\beta_c$ .  $A_{4\pi}/A_{2\pi}$  features for high frequency is found to collapse onto a single line with a value related to  $r$ . (b) Simulation results for different  $C$ . In lower frequency, we can see the crossover regime in which  $f_J/2$  maybe enhanced beyond the amplitude of the  $f_J$  feature depending on the value of  $\beta_c$ . (c) Simulation results for different values of ratio  $r$ . When  $r$  becomes small, the amplitude ratio in high frequency is suppressed much lower than  $r$ .

proximity gap of  $\Delta' = 180 \mu\text{eV}$  at  $V_g = 80 \text{ V}$  we predict  $i_{4\pi} \sim e\Delta'/\hbar \sim 44 \text{ nA}$ <sup>54</sup>. We estimate  $I_{\text{sw}} = 672 \text{ nA}$  so that the ratio  $r$  is estimated as 0.07. We expect much more than 20 times weaker emission feature at  $f_J/2$  compared with  $f_J$  for the high frequency regime considering the results of Fig. 6. Considering our results, we determine that the noise level is enough to hide the emission amplitude  $A_{4\pi}$ . This is probably due to the large capacitance which makes all the signal including the  $4\pi$  periodic emission weaker than the noise level. So far, we have only discussed the Josephson emission. However, in the Shapiro step measurement and the Josephson emission measurement similar conditions are necessary for observation of the  $4\pi$  periodic component<sup>53</sup>.

## CONCLUSION

We fabricated gate-tunable JJs on molecular beam epitaxy grown  $(\text{Bi}_{1-x}\text{Sb}_x)_2\text{Te}_3$  topological insulator. The supercurrent and normal resistance were controlled by a back-gate voltage demonstrating ambipolar transport. The  $I_{\text{sw}}R_n$  product was also gate voltage dependent and exhibits a pronounced dip feature near the Charge neutral point. This  $I_{\text{sw}}R_n$  behavior can be ascribed to the specular Andreev reflection at the boundaries of electron-hole puddles. Finally, by using gate tunable JJs, we carried out measurement of the ac Josephson effect. By radiating the JJs with microwaves, we observed a conventional pattern of Shapiro steps. We also observe the signature of conventional Josephson emission.

From our results and the support of simulation, it is most probable that small  $r$  and large parallel capacitance are the reasons why we are unable to observe the fractional ac Josephson effect. This indicates that  $\text{SrTiO}_3$  maybe a poor substrate choice for studying the fractional ac Josephson effect due to the high parallel capacitance. **The dielectric constant of  $\text{SrTiO}_3$  in low temperature is  $\simeq 20000$ , and the thickness of  $\text{SrTiO}_3$  used in our experiment is 0.5 mm. With the same device design, the  $\text{SrTiO}_3$  substrate is equivalent to a heavily doped Si substrates covered with 100 nm-thick  $\text{SiO}_2$ . This implies that the parallel capacitance does not become remarkably smaller as far as substrates with the back gate structure are used. Thus we suspect that such substrates are not suitable for observing missing step.**

## ACKNOWLEDGEMENTS

This work was partially supported by a JSPS Grant-in-Aid for Scientific Research (B) (No. JP18H01813), a JSPS Grant-in-Aid for Scientific Research (S) (Grant Nos. JP26220710, JP19H05610), JST CREST (Grant No. JPMJCR15N2), JST PREST (Grant No. JPMJPR18L8), the JSPS Program for Leading Graduate Schools (MERIT) from JSPS, JSPS Research Fellowship for Young Scientists (Grant Nos. JP18J14172, JP19J13867), NSF-CAREER award (DMR-1847811), the Gordon and Betty Moore Foundation's EPiQS Initiative, and Grant GBMF9063 to C.C..

\* sadashige.matsuo@riken.jp

† tarucha@riken.jp

- <sup>1</sup> E. Majorana, *Nuovo Cimento* **14**, 171 (1937).
- <sup>2</sup> A. Y. Kitaev, *Physics-Uspekhi* **44**, 131 (2001).
- <sup>3</sup> A. Y. Kitaev, *Annals of Physics* **303**, 2 (2003).
- <sup>4</sup> D. A. Ivanov, *Physical review letters* **86**, 268 (2001).
- <sup>5</sup> C. Nayak, S. H. Simon, A. Stern, M. Freedman, and S. D. Sarma, *Reviews of Modern Physics* **80**, 1083 (2008).
- <sup>6</sup> R. M. Lutchyn, J. D. Sau, and S. D. Sarma, *Physical review letters* **105**, 077001 (2010).
- <sup>7</sup> Y. Oreg, G. Refael, and F. von Oppen, *Physical review letters* **105**, 177002 (2010).
- <sup>8</sup> L. Fu and C. L. Kane, *Physical review letters* **100**, 096407 (2008).
- <sup>9</sup> L. Fu and C. L. Kane, *Physical Review B* **79**, 161408 (2009).
- <sup>10</sup> V. Mourik, K. Zuo, S. M. Frolov, S. R. Plissard, E. P. A. M. Bakkers, and L. P. Kouwenhoven, *Science* **336**, 1003 (2012).
- <sup>11</sup> A. Das, Y. Ronen, Y. Most, Y. Oreg, M. Heiblum, and H. Shtrikman, *Nature Physics* **8**, 887 (2012).
- <sup>12</sup> M. T. Deng, C. L. Yu, G. Y. Huang, M. Larsson, P. Caroff, and H. Q. Xu, *Nano letters* **12**, 6414 (2012).

- <sup>13</sup> S. M. Albrecht, A. P. Higginbotham, M. Madsen, F. Kuemmeth, T. S. Jespersen, J. Nygård, P. Krogstrup, and C. M. Marcus, *Nature* **531**, 206 (2016).
- <sup>14</sup> L. P. Rokhinson, X. Liu, and J. K. Furdyna, *Nature Physics* **8**, 795 (2012).
- <sup>15</sup> J. Wiedenmann, E. Bocquillon, R. S. Deacon, S. Hartinger, O. Herrmann, T. M. Klapwijk, L. Maier, C. Ames, C. Brüne, C. Gould, *et al.*, *Nature communications* **7**, 10303 (2016).
- <sup>16</sup> E. Bocquillon, R. S. Deacon, J. Wiedenmann, P. Leubner, T. M. Klapwijk, C. Brüne, K. Ishibashi, H. Buhmann, and L. W. Molenkamp, *Nature nanotechnology* **12**, 137 (2017).
- <sup>17</sup> R. S. Deacon, J. Wiedenmann, E. Bocquillon, F. Domínguez, T. M. Klapwijk, P. Leubner, C. Brüne, E. M. Hankiewicz, S. Tarucha, K. Ishibashi, *et al.*, *Physical Review X* **7**, 021011 (2017).
- <sup>18</sup> K. Le Calvez, L. Veyrat, F. Gay, P. Plaidoux, C. B. Winkelmann, H. Courtois, and B. Sacépé, *Communications Physics* **2**, 4 (2019).
- <sup>19</sup> R. Yano, M. Koyanagi, H. Kashiwaya, K. Tsumura, H. T. Hirose, T. Sasagawa, Y. Asano, and S. Kashiwaya, *arXiv:1805.10435 [cond-mat.supr-con]* (2018).
- <sup>20</sup> P. Schüffelgen, D. Rosenbach, C. Li, T. W. Schmitt, M. Schleenvoigt, A. R. Jalil, S. Schmitt, J. Kölzer, M. Wang, B. Bennemann, *et al.*, *Nature nanotechnology*

- 14**, 825 (2019).
- <sup>21</sup> D. Laroche, D. Bouman, D. J. van Woerkom, A. Prutski, C. Murthy, D. I. Pikulin, C. Nayak, R. J. J. van Gulik, J. Nygård, P. Krogstrup, L. P. Kouwenhoven, and A. Geresdi, *Nature Communications* **10**, 245 (2019).
  - <sup>22</sup> S. Nadj-Perge, I. K. Drozdov, J. Li, H. Chen, S. Jeon, J. Seo, A. H. MacDonald, B. A. Bernevig, and A. Yazdani, *Science* **346**, 602 (2014).
  - <sup>23</sup> G. C. Ménard, S. Guissart, C. Brun, R. T. Leriche, M. Trif, F. Debontridder, D. Demaille, D. Roditchev, P. Simon, and T. Cren, *Nature communications* **8**, 2040 (2017).
  - <sup>24</sup> C. Li, J. C. de Boer, B. de Ronde, S. V. Ramankutty, E. van Heumen, Y. Huang, A. de Visser, A. A. Golubov, M. S. Golden, and A. Brinkman, *Nature materials* **17**, 875 (2018).
  - <sup>25</sup> A.-Q. Wang, C.-Z. Li, C. Li, Z.-M. Liao, A. Brinkman, and D.-P. Yu, *Physical review letters* **121**, 237701 (2018).
  - <sup>26</sup> A. R. Akhmerov, J. Nilsson, and C. W. J. Beenakker, *Physical Review Letters* **102** (2009).
  - <sup>27</sup> S. Park and P. Recher, *Physical review letters* **115**, 246403 (2015).
  - <sup>28</sup> P. Schüffelgen, D. Rosenbach, C. Li, T. Schmitt, M. Schleenvoigt, A. R. Jalil, J. Kölzer, M. Wang, B. Benne- mann, U. Parlak, *et al.*, arXiv:1711.01665 [cond-mat.supr- con] (2017).
  - <sup>29</sup> S. Park, H.-S. Sim, and P. Recher, arXiv:1812.09573 [cond- mat.mes-hall] (2018).
  - <sup>30</sup> J. Zhang, C.-Z. Chang, Z. Zhang, J. Wen, X. Feng, K. Li, M. Liu, K. He, L. Wang, X. Chen, *et al.*, *Nature commu- nications* **2**, 574 (2011).
  - <sup>31</sup> D.-X. Qu, Y. S. Hor, J. Xiong, R. J. Cava, and N. P. Ong, *Science* **329**, 821 (2010).
  - <sup>32</sup> R. Yoshimi, A. Tsukazaki, Y. Kozuka, J. Falson, K. S. Takahashi, J. G. Checkelsky, N. Nagaosa, M. Kawasaki, and Y. Tokura, *Nature communications* **6**, 6627 (2015).
  - <sup>33</sup> S. Ghatak, O. Breunig, F. Yang, Z. Wang, A. A. Taskin, and Y. Ando, *Nano letters* **18**, 5124 (2018).
  - <sup>34</sup> H. J. Suominen, J. Danon, M. Kjaergaard, K. Flensberg, J. Shabani, C. J. Palmstrøm, F. Nichele, and C. M. Mar- cus, *Physical Review B* **95**, 035307 (2017).
  - <sup>35</sup> J. Gu, W. Cha, K. Gamo, and S. Namba, *Journal of Ap- plied Physics* **50**, 6437 (1979).
  - <sup>36</sup> B. Sacépé, J. B. Oostinga, J. Li, A. Ubaldini, N. J. G. Couto, E. Giannini, and A. F. Morpurgo, *Nature commu- nications* **2**, 575 (2011).
  - <sup>37</sup> D. Jeong, J.-H. Choi, G.-H. Lee, S. Jo, Y.-J. Doh, and H.-J. Lee, *Physical Review B* **83**, 094503 (2011).
  - <sup>38</sup> F. Miao, W. Bao, H. Zhang, and C. N. Lau, *Solid State Communications* **149**, 1046 (2009).
  - <sup>39</sup> H. B. Heersche, P. Jarillo-Herrero, J. B. Oostinga, L. M. K. Vandersypen, and A. F. Morpurgo, *Nature* **446**, 56 (2007).
  - <sup>40</sup> X. Du, I. Skachko, and E. Y. Andrei, *Physical Review B* **77**, 184507 (2008).
  - <sup>41</sup> J.-H. Choi, G.-H. Lee, S. Park, D. Jeong, J.-O. Lee, H.-S. Sim, Y.-J. Doh, and H.-J. Lee, *Nature communications* **4**, 2525 (2013).
  - <sup>42</sup> E. H. Hwang, S. Adam, and S. D. Sarma, *Physical review letters* **98**, 186806 (2007).
  - <sup>43</sup> V. V. Cheianov, V. I. Falko, B. L. Altshuler, and I. L. Aleiner, *Physical review letters* **99**, 176801 (2007).
  - <sup>44</sup> J. Martin, N. Akerman, G. Ulbricht, T. Lohmann, J. H. Smet, K. Von Klitzing, and A. Yacoby, *Nature physics* **4**, 144 (2008).
  - <sup>45</sup> Y. Zhang, V. W. Brar, C. Girit, A. Zettl, and M. F. Crommie, *Nature Physics* **5**, 722 (2009).
  - <sup>46</sup> K. Komatsu, C. Li, S. Autier-Laurent, H. Bouchiat, and S. Guéron, *Physical Review B* **86**, 115412 (2012).
  - <sup>47</sup> C. W. J. Beenakker, *Physical review letters* **97**, 067007 (2006).
  - <sup>48</sup> H. Beidenkopf, P. Roushan, J. Seo, L. Gorman, I. Drozdov, Y. S. Hor, R. J. Cava, and A. Yazdani, *Nature Physics* **7**, 939 (2011).
  - <sup>49</sup> L. Majidi and R. Asgari, *Physical Review B* **93**, 195404 (2016).
  - <sup>50</sup> See Supplemental Material at [URL will be inserted by publisher].
  - <sup>51</sup> F. Domínguez, F. Hassler, and G. Platero, *Physical Re- view B* **86**, 140503 (2012).
  - <sup>52</sup> J. Picó-Cortés, F. Domínguez, and G. Platero, *Physical Review B* **96**, 125438 (2017).
  - <sup>53</sup> F. Domínguez, O. Kashuba, E. Bocquillon, J. Wieden- mann, R. S. Deacon, T. M. Klapwijk, G. Platero, L. W. Molenkamp, B. Trauzettel, and E. M. Hankiewicz, *Phys- ical Review B* **95**, 195430 (2017).
  - <sup>54</sup> C. W. J. Beenakker and H. Van Houten, *Physical review letters* **66**, 3056 (1991).